Evaluating reproducibility and subject-specificity of microstructure-informed connectivity

Philipp J. Koch [a,b,c,d,1], Gabriel Girard [e,f,g,1,*], Julia Brügger [a,b], Andéol G. Cadic-Melchior [a,b], Elena Beanato [a,b], Chang-Hyun Park [a,b], Takuya Morishita [a,b], Maximilian J. Wessel [a,b,h], Marco Pizzolato [g,i], Erick J. Canales-Rodríguez [g], Elda Fischi-Gomez [g,j], Simona Schiavi [k,l], Alessandro Daducci [k], Gian Franco Piredda [f,g,m], Tom Hilbert [f,g,m], Tobias Kober [f,g,m], Jean-Philippe Thiran [e,f,g,1], Friedhelm C. Hummel [a,b,n,1]

[a] *Defitech Chair of Clinical Neuroengineering, Center for Neuroprosthetics (CNP) and Brain Mind Institute (BMI), École Polytechnique Fédérale de Lausanne (EPFL), 1202 Geneva, Switzerland*
[b] *Defitech Chair of Clinical Neuroengineering, Center for Neuroprosthetics (CNP) and Brain Mind Institute (BMI), École Polytechnique Fédérale de Lausanne (EPFL Valais), Clinique Romande de Réadaptation, 1951 Sion, Switzerland*
[c] *Department of Neurology, University of Lübeck, 23562 Lübeck, Germany*
[d] *Center of Brain, Behavior and Metabolism (CBBM), University of Lübeck, 23562 Lübeck, Germany*
[e] *CIBM Center for Biomedical Imaging, Switzerland*
[f] *Radiology Department, Centre Hospitalier Universitaire Vaudois and University of Lausanne, Lausanne, Switzerland*
[g] *Signal Processing Laboratory (LTS5), École Polytechnique Fédérale de Lausanne (EPFL), Switzerland*
[h] *Department of Neurology, Julius-Maximilians-University Würzburg, Würzburg, Germany*
[i] *Department of Applied Mathematics and Computer Science, Technical University of Denmark, Kgs. Lyngby, Denmark*
[j] *Translational Machine Learning Lab, Radiology Department, Centre Hospitalier Universitaire Vaudois and University of Lausanne, Lausanne, Switzerland*
[k] *Diffusion Imaging and Connectivity Estimation (DICE) Lab, Department of Computer Science, University of Verona, Verona, Italy*
[l] *Department of Neuroscience, Rehabilitation, Ophthalmology, Genetics, Maternal and Child Health (DINOGMI), University of Genoa, Genoa, Italy*
[m] *Advanced Clinical Imaging Technology, Siemens Healthcare AG, Lausanne, Switzerland*
[n] *Clinical Neuroscience, University Hospital of Geneva (HUG), Geneva, Switzerland*

ARTICLE INFO

ABSTRACT

Tractography enables identifying and evaluating the healthy and diseased brain's white matter pathways from diffusion-weighted magnetic resonance imaging data. As previous evaluation studies have reported significant false-positive estimation biases, recent microstructure-informed tractography algorithms have been introduced to improve the trade-off between specificity and sensitivity. However, a major limitation for characterizing the performance of these techniques is the lack of ground truth brain data. In this study, we compared the performance of two relevant microstructure-informed tractography methods, *SIFT2* and *COMMIT*, by assessing the subject specificity and reproducibility of their derived white matter pathways. Specifically, twenty healthy young subjects were scanned at eight different time points at two different sites. Subject specificity and reproducibility were evaluated using the whole-brain connectomes and a subset of 29 white matter bundles. Our results indicate that although the raw tractograms are more vulnerable to the presence of false-positive connections, they are highly reproducible, suggesting that the estimation bias is subject-specific. This high reproducibility was preserved when microstructure-informed tractography algorithms were used to filter the raw tractograms. Moreover, the resulting track-density images depicted a more uniform coverage of streamlines throughout the white matter, suggesting that these techniques could increase the biological meaning of the estimated fascicles. Notably, we observed an increased subject specificity by employing connectivity pre-processing techniques to

reduce the underlaying noise and the data dimensionality (using principal component analysis), highlighting the importance of these tools for future studies. Finally, no strong bias from the scanner site or time between measurements was found. The largest intraindividual variance originated from the sole repetition of data measurements (inter-run).

1. Introduction

Diffusion-weighted magnetic resonance imaging (DW-MRI) and tractography algorithms enable the indirect in-vivo assessment of white matter fascicles' trajectories and properties in the human brain. This has revolutionized neuroscience, allowing researchers to move away from post mortem analysis and perform their studies non-invasively (Assaf et al., 2017). These techniques have become a fundamental part of systems and translational neuroscience. From the measurements of the displacement of water molecules for specific gradient directions, it is possible to obtain the 3-dimensional (3D) reconstruction of white matter fascicles' trajectories and the description of whole-brain connectomes. Moreover, the local qualitative and quantitative examination of microstructure offers unique possibilities to address various questions in clinics and research. For instance, the study of temporal changes of white matter structures allows the assessment of plastic changes and factors like degeneration persistent in healthy and neurological disease (Sagi et al., 2012). Longitudinal evaluations of the white matter hereby reveal insights into, e.g., learning processes (Scholz et al., 2009) or white matter reorganization after focal brain lesions, such as stroke (Koch et al., 2021; for review: Koch and Hummel, 2017). Still, those techniques encompass multiple steps vulnerable to noise, uncertainties, and approximations that affect the interpretation of findings.

The main critical drawback of fibre tracking techniques is the reconstruction of a significant number of invalid tracts, i.e., false positives. Interestingly, a recent international tractography challenge revealed that a high percentage of false positives (e.g. 64% of the reconstructed bundles) could be obtained even when the ground truth fibre orientation distribution functions (ODFs) are used (Maier-Hein et al., 2017). Thus, new innovative methods to improve the trade-off between sensitivity and specificity are needed (Schilling et al., 2019) by identifying and filtering out the spurious streamlines. Another important limitation is that the structural connectivity matrix estimated by commonly used tractography algorithms remains qualitative, with an unknown biological meaning, because the density of reconstructed connections does not reflect the underlying white matter fibre density (Smith et al., 2015). To address the limitations, microstructure-informed tractography methods were introduced, where each generated streamline is evaluated by its consistency in relation to the whole tractogram and the measured DW-MRI data. Two state-of-the-art methods are the spherical-deconvolution informed filtering of tractograms (SIFT2; SIFT; Smith et al., 2015, 2013a) and convex optimization modelling for microstructure-informed tractography (COMMIT; Daducci et al., 2014b). Both approaches differ on how the consistency of each streamline is measured. In SIFT2, the optimal weighted set of streamlines is determined so that the resulting weighted local orientation density of streamlines is as close as possible to the fibre ODFs estimated using spherical deconvolution (Tournier et al., 2007). The authors hypothesized that this postprocessing step permits using the sum of streamline weights as a biological marker of connection density (Smith et al., 2015b). Similarly, COMMIT solves a global inverse problem to estimate a weight for each streamline by assuming a generative multi-compartment microstructure model for the measured data, which usually includes the intra- and extra-axonal spaces and free water. The global optimization problem is solved by using constant microstructure properties throughout each streamline trajectory (Barakovic et al., 2021a, 2021b, 2016; Daducci et al., 2014b, 2013; Ocampo-Pineda et al., 2021a; Pestilli et al., 2014; Reisert et al., 2014; Schiavi et al., 2020a; Sherbondy et al., 2010; Smith et al., 2013b; Smith et al., 2015). The generated signals are projected to the 3D voxel-space by considering the length of their segments crossing each voxel, which is assumed to be proportional to the local volume fraction (Daducci et al., 2013, 2014b). A linear regression model is then designed to decompose the measured data as a linear combination of the generated signals. The estimated weights, thus, quantify the signal fraction of each streamline in the measured data and assign a biological meaning to each connection as a surrogate of the axonal cross-sectional area (Daducci et al., 2014b). Those streamlines with trajectories not supported by the measured data have weights close to zero and thus are considered false positives. Like SIFT2, COMMIT can correct for overrepresented or underrepresented streamlines (due to tractography biases) by adjusting their weights (Ocampo-Pineda et al., 2021a; Schiavi et al., 2020a). Although previous studies found that these microstructure-informed tractography algorithms can significantly alter the estimated white matter network topology (Frigo et al., 2020; Smith et al., 2015b), their stability, reproducibility, and accuracy have not been compared. This is a crucial step before its use for answering neuroscientific and clinical questions. Thus, this study evaluates the reproducibility, repeatability, and subject specificity of microstructure-informed tractography methods considering the site, session, and run effects. This was done by collecting DW-MRI data from 20 healthy participants in two scanners located at different sites during two consecutive scanning sessions and two distinct time points, for a total of 160 datasets (eight per participant).

In this regard, reproducibility defines consequent results in the reconstruction of white matter over multiple measurements of one subject, regardless of the site, whereas repeatability defines the stability of the results in immediate repetition at the same scanner. This was estimated within the given study by the intraindividual and interindividual Bray Curtis dissimilarity as well as the intraclass correlation coefficient (ICC). The subject specificity was evaluated by the accuracy of identifying all eight datasets belonging to one subject.

2. Material and methods

2.1. Participants

Twenty healthy subjects (Age: 27 (24 – 33 years old, +/- 3 years SEM), nine female) were enrolled in the study. Magnetic resonance imaging (MRI) was performed at two sites (Geneva: G, Sion: S) at two different time points (sessions). At each session, two independent repetitions of the neuroimaging protocols were acquired (run), ending up in 8 datasets per participant. Between the runs, subjects exited the scanner and were then repositioned, followed by a new shimming. For each session, a single 3D MPRAGE was acquired. The mean elapsed time between intra-site and inter-site repetitions was 16 days (+/- 10 days) and 29 days (+/- 17 days), respectively. All subjects were right-handed and had no neuropsychiatric diseases or contraindications for MRI. Written informed consent was obtained from each participant following the Declaration of Helsinki. The ethical approval was obtained from the cantonal ethics committee Vaud, Switzerland (project number: 2018–01355).

2.2. Magnetic resonance imaging data acquisition

At both sites (G and S), structural T1-weighted and diffusion-weighted MRI data were acquired at 3T (MAGNETOM Prisma scanner, Siemens Healthcare, Erlangen, Germany) and employed the same acquisition protocol. DW-MRI data were acquired using a pulsed gradient spin echo sequence with the following parameters: TR = 5000 ms;

TE = 77 ms; slices = 84; field of view = 234×234 mm^2; voxel resolution = $1.6 \times 1.6 \times 1.6$ mm^3; slice thickness of 1.6 mm; readout bandwidth = 1630 Hz/pixels; 64-channel head coil; GRAPPA acceleration factor =3. Seven T2-weighted images without diffusion weighting (b0; $b = 0$ s/mm^2) were acquired, including one in opposite phase encoding direction. A total of 101 images with noncollinear diffusion gradient directions distributed equidistantly over the half-sphere and covering 5 diffusion-weighting gradient strengths were obtained (b-values = [300, 700, 1000, 2000, 3000] s/mm^2; shell-samples = [3, 7, 16, 29, 46]). In addition, T1-weighted images were acquired using a 3D MPRAGE sequence with the following acquisition parameters: TR = 2300 ms; Inversion Time = 7.1 ms; TE = 2.96 ms; flip angle = 9°; slices = 192; voxel size =$1 \times 1 \times 1$ mm^3, field of view = 256×256 mm^2.

2.3. Image analysis

The DW-MRI images were corrected for Gibbs ringing artefacts using *MRtrix3* (Kellner et al., 2016; Tournier et al., 2019) and for motion, field inhomogeneity, susceptibility-induced off-resonance field, and eddy currents using the *FSL topup* and *eddy* (Andersson et al., 2003; Andersson and Sotiropoulos, 2016; Smith et al., 2004). Subsequently, the images were corrected for spatial intensity variations using *FSL FAST* (Zhang et al., 2001). Multi-shell multi-tissue constrained spherical deconvolution (Jeurissen et al., 2014) was used to estimate the fibre ODF within each voxel. Whole-brain probabilistic tractography was performed using the second-order integration over fibre orientation distribution (iFOD2; Tournier et al., 2019), initiating streamlines in all voxels of the white matter. For each dataset, 5 million streamlines were generated, from which all streamlines with both endpoints in the individual cortical or subcortical brain masks were selected using the *DIPY* software package (Garyfallidis et al., 2014). Moreover, the diffusion tensors and corresponding Mean Diffusivity (MD) and Fractional Anisotropy (FA) maps were estimated using *MRtrix3* (Tournier et al., 2019). Tissue partial volume estimates were obtained from the T1-weighted image using the *FSL FAST* (Zhang et al., 2001) and *BET* (Smith, 2002) methods. The T1-weighted image was registered to the average b0 image using *FSL FLIRT* (Jenkinson et al., 2002) and *FNIRT* (Andersson et al., 2010).

2.4. Whole-brain connectome estimation

For the cortical parcellation, the Destrieux atlas (74 areas per hemisphere) was used, available in *FreeSurfer* (Destrieux et al., 2010; Fischl et al., 2004, 2002; Iglesias et al., 2015). Additionally, subcortical areas (thalamus, caudate, putamen. hippocampus, amygdala), the cerebellum, and a subdivision of the brainstem (midbrain, pons, medulla) were added, yielding 163 cortical and subcortical areas. Estimated streamlines by the whole-brain tractography were used to analyse structural connectivity between those 163 areas, i.e. the structural connectome. This resulted in a structural connectivity analysis of 13,203 pairs of areas. Connectomes were generated in five different fashions. First, we estimated the fraction of streamlines connecting two regions of interest (i.e., the number of streamlines between all pairs of regions divided by the total number of streamlines). Second, tractograms were filtered based on the underlying white matter fibre densities using *SIFT2* (Smith et al., 2015), implemented in *MRtrix3* (Kellner et al., 2016; Tournier et al., 2019). Third and forth, each streamline was weighted by using *COMMIT* (Daducci et al., 2014b) using two diffusion models: the ball and stick (*COMMIT B&S*) and Stick-Zeppelin-Ball (*COMMIT SZB*). The stick compartment models the intra-axonal water with parallel diffusivity fixed to 1.7 µm^2/ms and no perpendicular diffusivity. The Ball compartment accounts for the isotropic extra-axonal water having a diffusivity of 1.7 µm^2/ms and the free water with diffusivity of 3.0 µm^2/ms (Alexander, 2008; Scholz et al., 2009). The Zeppelin compartment models the anisotropic extra-axonal water with parallel and perpendicular diffusivities fixed to 1.7 µm^2/ms and 0.51 µm^2/ms (Alexander, 2008), respectively. Fifth, tractograms were filtered using the *COMMIT* method

with bundle sparsity constraints (*COMMIT2*; Schiavi et al., 2020a). This method aims at solving the optimization problem using prior knowledge of the white matter anatomy. As such, streamlines are grouped in bundles based on their endpoints connectivity, and *COMMIT2* optimized the streamline weights such that they both explain the data while also minimizing the number of bundles (e.i. maximizing the number of zeros in the connectome). *COMMIT2* was parametrised to use the volume fraction model (Schiavi et al., 2020a). The intra-cellular volume fraction map was obtained using the Spherical Mean Technique method (Kaden et al., 2015) available at https://github.com/ekaden/smt (*fitmcmicro* command). Streamlines were grouped in bundles using the 163 cortical and subcortical areas obtained from the Destrieux atlas described above (Destrieux et al., 2010). The *COMMIT2* group sparsity regularisation parameter was set to 0.5×10^{-10}, reducing the average connectome density (non-zero connections) from 70.2% to 43.6% (the raw tractogram connectomes have an average density of 89.4%).

2.5. Principal component analysis of whole-brain connectomes

The 13,203 connections in each dataset compromise further statistical analyses by redundancy and collinearity. This is why we have introduced a further step of connectome reconstruction. Principal Component Analysis (PCA) was employed to extract eigenvectors explaining variance in the data with 160 samples x 13.203 connections. The eigenvectors and eigenvalues were chosen to account for 10% - 100% of the variance explained. This was performed for the five connectome constructions (i.e., raw and filtered tractograms using *SIFT2, COMMIT B&S/SZB* and *COMMIT2*). Afterwards, for each step of variance explained (10–90%), the respective number of principal components were applied to reconstruct the connectomes in the original space. These analyses were performed to keep the individual connectomes in the native space while reducing their intrinsic dimensionality, diminishing redundant and colinear entries of the connectome by means of PCA eigenvectors. These newly arrived PCA reduced connectomes were fed into further analysis of reproducibility.

2.6. Bundle connectivity vector estimation

Twenty-nine white matter fascicles of the human brain were automatically segmented using a white matter query language (Wassermann et al., 2016). See the supplementary material for more details about the selected white matter fascicle definition (queries). The areas used for the anatomical definition of the white matter bundles (*wmparc* image) were obtained from *FreeSurfer* (Fischl et al., 2002) and coregistered to the diffusion space using *FSL FLIRT* (Jenkinson et al., 2002) and *FNIRT* (Andersson et al., 2010).

The following white matter fascicles were reconstructed: right and left Arcuate Fasciculus (frontotemporal, frontoparietal, parietotemporal), right and left Cingulum, right and left Fornix, right and left Inferior Fronto-Occipital Fasciculus, right and left Optic Radiation, right and left Pyramidal Tract, right and left Superior Longitudinal Fasciculus (I, II, II), right and left Uncinate Fasciculus, Corpus Callosum (anterior, mid anterior, central, mid posterior, posterior). The structural connectivity of each white matter fascicle was estimated in five different ways, similar to the whole brain connectomes being the fraction of streamlines, filtered streamlines using *SIFT2* and weighted streamlines using the three *COMMIT* method variants. This created five vectors of 29 values, termed bundle connectivity vector.

2.7. Diffusion tensor imaging

The white matter parcellation of every individual dataset was obtained using *FreeSurfer* (Fischl et al., 2002), creating 148 parcellated regions within the white matter. For each parcellated region, the mean values of the orientationally invariant scalar maps (MD and FA) were estimated for every individual dataset, resulting in two vectors with 148

values representing the areas of white matter parcellation, one for FA and one for MD values.

2.8. Tract-density imaging maps

Track-density imaging (TDI; Calamante et al., 2010) maps were created using *MRtrix3* (Tournier et al., 2019) for the five evaluated tractograms (raw and filtered tractograms). TDI maps are built by counting the number of streamlines intersecting each voxel. For microstructure-informed tractography methods, the maps were created by summing the weights of the streamlines intersecting each voxel. All individual datasets were registered to the MNI standard space using *FSL FLIRT* (Jenkinson et al., 2002) and *FNIRT* (Andersson et al., 2010). Subsequently, the individual datasets were voxelwise transformed to z-scores with positive values indicating voxels with high tract density compared to the whole brain and the average map of all individual datasets was estimated.

2.9. Connectome reproducibility and subject-specificity

2.9.1. Dissimilarity measure

To compare connectomes, bundle connectivity vectors and tensor map vectors, we used the Bray–Curtis dissimilarity index (Bray and Curtis, 1957), defined as:

$$\frac{\Sigma \left| C1_{ij} - C2_{ij} \right|}{\Sigma \left| C1_{ij} + C2_{ij} \right|},$$

where C1 and C2 are two non-zero connectomes or bundle connectivity vectors, i and j are the line and column index, respectively. The Bray-Curtis dissimilarity index value ranges between 0 and 1.

2.9.2. Seven-nearest-neighbour clustering

There are eight datasets for each of the 20 participants of the study. For each dataset and connectivity metric (connectomes, bundle connectivity vectors, tensor map vectors), the seven datasets with the lowest Bray-Curtis dissimilarity to this dataset were selected. amongst them, we identified how many datasets match that participant, producing a score between 0 and 7. This was repeated for all 160 datasets, resulting in a clustering score between 0 and 1120 for each connectivity method. A good performing algorithm should separate participants (producing high inter-individual Bray-Curtis dissimilarity values) and be reproducible for datasets acquired from the same participant (with low intraindividual Bray-Curtis dissimilarity values).

2.9.3. Intraclass correlation coefficients

As a further measurement of data reproducibility, we have used the intraclass correlation coefficient (ICC) implemented in R-studio (Smith, 1957). For the raw tractograms as well as the filtered connectomes and their respective PCA reduced connectomes, the ICC was calculated for every entry in the connectome individually. Afterwards, the percentage of entries >0.75 and >0.9 representing very good and excellent reproducibility were reported. Connectome entries with non-zero in all 160 datasets were considered for this analysis. Thus, the number of total entries varies between methods, and PCA reduced connectomes.

2.9.4. Distribution of fascicle connectivity

For every dataset and each of the 29 white mater fascicles, the distribution of structural connectivity estimates within the 20 subjects was estimated and analysed with the Shapiro-Wilk test for evaluating whether the estimates deviate from the normal distribution. This was performed for the raw and filtered tractograms. The percentage of datasets following a normal distribution was compared.

2.10. Repeated measure ANOVA

For all individual dataset the average dissimilarity to all other datasets was calculated. For each connectome reconstruction (Raw tractogram, *SIFT2*, *COMMIT B&S/SZB*, *COMMIT2*) one separate RM-ANOVA was conducted comparing values of mean dissimilarity between sites, sessions and runs with factors being: SION, GENEVA; Session1, Session2, Run1, Run2.

2.11. Data availability statement

Data can be made available upon reasonable request.

3. Results

3.1. Dissimilarity between connectomes and connectivity vectors

We have acquired 8 datasets of 20 individuals over a short period using the same acquisition parameters (160 datasets). The structural connectivity estimated from these datasets for one individual should show strong similarity as no major changes should have taken place amongst scans. Moreover, the structural connectivity should show subject-specificity and thus an increased dissimilarity amongst subjects. Fig. 1 shows the Bray-Curtis dissimilarity index between all pairs of connectomes and bundle connectivity vectors. The Bray-Curtis dissimilarity index for the diffusion tensor map is shown in the supplementary material. The structural connectivity values were computed from the raw tractogram (first column), *SIFT2*wt (second column), *COMMIT B&S/SZB* wt (third and forth columns), and COMMIT2 wt (fifth column). Datasets are ordered by subjects, sites (site G, then site S), sessions, and runs. The colours codify the Bray-Curtis dissimilarity amongst all datasets and methods. The 8×8 squares visible around the diagonal (blue) show the intraindividual dissimilarities, and the off-diagonal values show the interindividual dissimilarities.

Table 1 reports the corresponding interindividual to intraindividual dissimilarity ratio (mean of the inter-subject dissimilarity over the mean of the intraindividual dissimilarity) and the seven-nearest-neighbour clustering performances of each method. The intraindividual dissimilarity ratio is equal for the whole-brain connectome using the raw tractogram or the filtered one with *SIFT2* at 2.32 and decreases to 1.92 and 1.96 for the *COMMIT B&S and COMMIT SZB* methods, respectively. The *COMMIT2* method showed the lowest results with 1.91. Their corresponding clustering performances are almost perfect for all methods. The microstructure-informed tractography methods have an increased intraindividual dissimilarity ratio compared to the raw tractogram when using the bundle connectivity vectors. Although the clustering performance decreases, it remains high, ranging from 79% (*COMMIT B&S*) to 86% (raw tractogram). The tensor map vectors show a lower intraindividual dissimilarity ratio of 2.05 and 1.84 when using the FA and MD, respectively. The clustering performance remains high when utilizing the tensor map vectors with a clustering performance of 95%.

Fig. 2 shows the whole-brain connectome interindividual to intraindividual dissimilarity (left) and clustering performances (right), decreasing the variance explained by the data after PCA filtering. The raw tractograms and *SIFT2*-filtered ones show similar results with an increase in ratio when decreasing the percent of variance explained. The maximum dissimilarity ratio is obtained using 80% of the variance and decreases as the percentage decreases further. The *COMMIT* method shows a different profile with a rapid increase at 80% of the variance, then a further increase as the percentage of the variance is reduced. Although the *COMMIT* method has a lower maximum ratio, the ratio is higher than that obtained for the raw tractogram and *SIFT2* method when using a 30% to 10% of the variance. The whole-brain connectome clustering performance is systematically higher for the raw tractogram, except for the *COMMIT* method when using 10% of variance explained by the data.
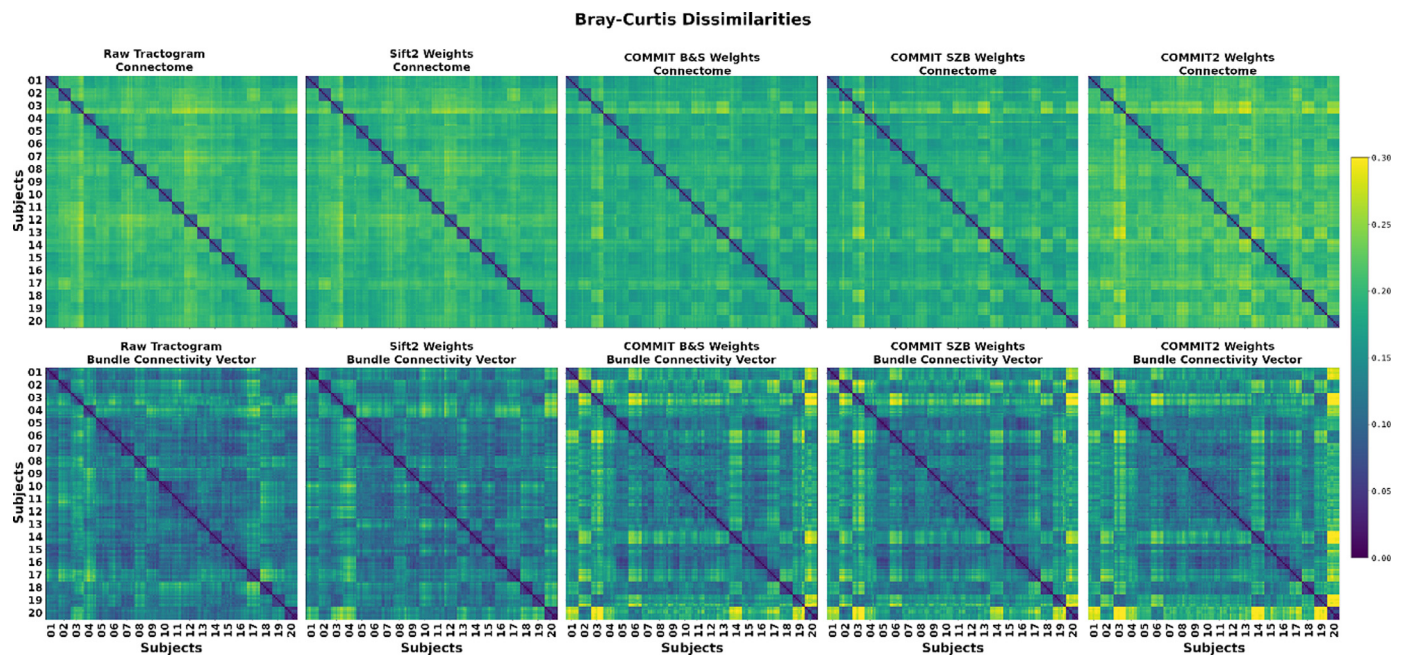
Fig. 1. Bray-Curtis dissimilarities between connectomes (first row) and bundle connectivity vectors (second row) computed from the raw tractograms (first column), and tractograms filtered by *SIFT2* (second column), and *COMMIT* (third, forth, fifth columns). Each subject has eight MRI datasets (two sites, two sessions per site, and two runs per session). The colours indicate the Bray-Curtis dissimilarity between all datasets and methods. The 8 × 8 blue squares around the main diagonal show the intraindividual dissimilarities, and other values depict the inter-subject dissimilarities.

Table 1

The ratio of interindividual to intraindividual dissimilarities measured by Bray-Curtis dissimilarity index and classification performances on the connectome, the bundle connectivity vectors, and the tensor map vectors. The dissimilarity index (between 0 and 1) represents how different two connectivity estimates are from each other. The clustering performance of 1120 indicates that each connectome or vector seventh-nearest-neighbours are from the same subject, i.e., any subject can identify the seven other datasets matching that subject.

Method		Interindividual to intraindividual dissimilarity ratio	Interindividual dissimilarity	Intraindividual dissimilarity	Clustering performance (max. 1120)
Whole-brain Connectome	**Raw Tractograms**	2.32	0.2024	0.0871	1120 (100%)
	SIFT2	2.32	0.1990	0.0858	1120 (100%)
	COMMIT B&S	1.92	0.1875	0.0976	1120 (100%)
	COMMIT SZB	1.96	0.1873	0.0956	1119 (99.9%)
	COMMIT2	1.91	0.2119	0.1110	1120 (100%)
Bundle Connectivity Vector	**Raw Tractogram**	2.32	0.1323	0.0570	964 (86.1%)
	SIFT2	2.45	0.1332	0.0543	948 (84.6%)
	COMMIT B&S	2.35	0.1542	0.0654	887 (79.2%)
	COMMIT SZB	2.44	0.1506	0.0618	922 (82.3%)
	COMMIT2	2.43	0.1532	0.0543	914 (81.6%)
Diffusion Tensor Map	**Average FA**	2.05	0.0456	0.0222	1067 (95.3%)
	Average MD	1.84	0.0343	0.0186	1066 (95.2%)

In Fig. 3, the percentage of connectome entries with ICC >0.75 and >0.9 are reported for all connectomes as well as the PCA reduced connectomes. The results show an excellent level of reproducibility for most of the PCA filtered connectomes using *COMMIT* wt with on average >60% of entries with an ICC score of >0.9. Using the raw tractogram as well as the *SIFT2* wt, there is a constant increase of entries with ICC>0.9 with a maximum at 80% variance explained with ca. 90% of entries. For all filtering methods, the ICC>0.9 decreased with 90% variance explained connectome, whilst remaining good reproducibility levels. Without any PCA applied, the ICC shows good reproducibility in ca. 45% of entries for the raw tractogram and the *SIFT2* weightedwt, 30% of entries in the *COMMIT2* weightedwt and 16 and 18% in the *COMMIT* weighted (*B&S, SZB*) connectomes.

Table 2 shows the results of the repeated measure ANOVA analysis comparing the mean intraindividual and interindividual dissimilarities between sites, sessions, and runs for the five studied whole-brain connectome methods separately. The comparison reveals no significant differences between sites, sessions and runs in the raw tractograms as well as the *COMMIT* weights; 7.1%, 1,8%, 2.9% and 3.2% of the data variance were explained by the factors site, session and run for the raw tractogram, the *COMMIT* (*B&S, SZB*) and *COMMIT2*wt, respectively. Using the *SIFT2*wt, the repeated measure ANOVA reveals a significant difference with 11.3% of variance explained. However, post hoc analysis showed no significant differences between the dissimilarities comparing sites, session and run individually, after correction for multiple comparisons.

Table 3 presents the average Bray-Curtis dissimilarity indices between datasets of the same individuals (intra-subject). Moreover, the average dissimilarity indices between datasets of the same individual, acquired at different sites (inter-site), or acquired at the same site but during different sessions (inter-session), or acquired at the same site and session but during different runs (inter-run) are reported. It is important to note that the inter-session dissimilarity also includes the dissimilarity inter-run. Similarly, the inter-site dissimilarity also includes the
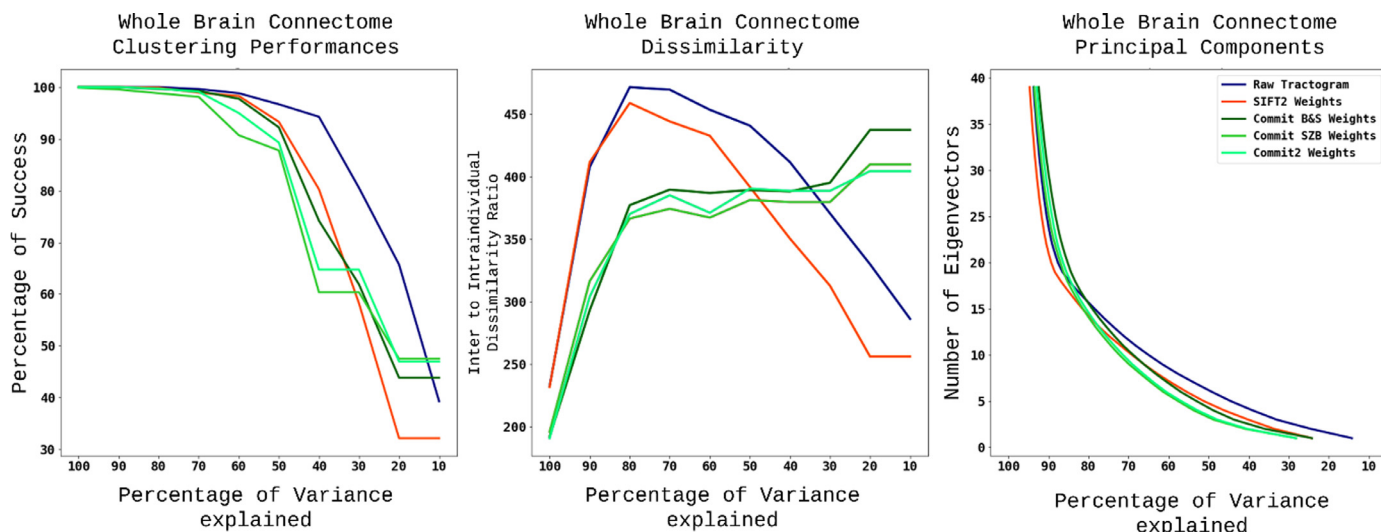
Fig. 2. Subject specificity in PCA reduced connectomes for the raw tractogram, the *SIFT2* and *COMMIT* methods. Percentage of success rate in seventh-nearest-neighbours clustering (left) as well as the interindividual to intraindividual dissimilarity ratio of whole-brain connectomes (middle) are shown accounting for various levels of explained variance by the principal Component Analysis (PCA). Using PCA the complex dataset of whole brain connectomes was reduced in dimensionality to a certain amount of eigenvectors explaining variance of the data ranging from 10 to 90% (right). Please note, that for 100% of variance, no PCA was performed, but the raw connectome and filtered connectomes are shown (same data as in e.g. Fig. 1, table 1).
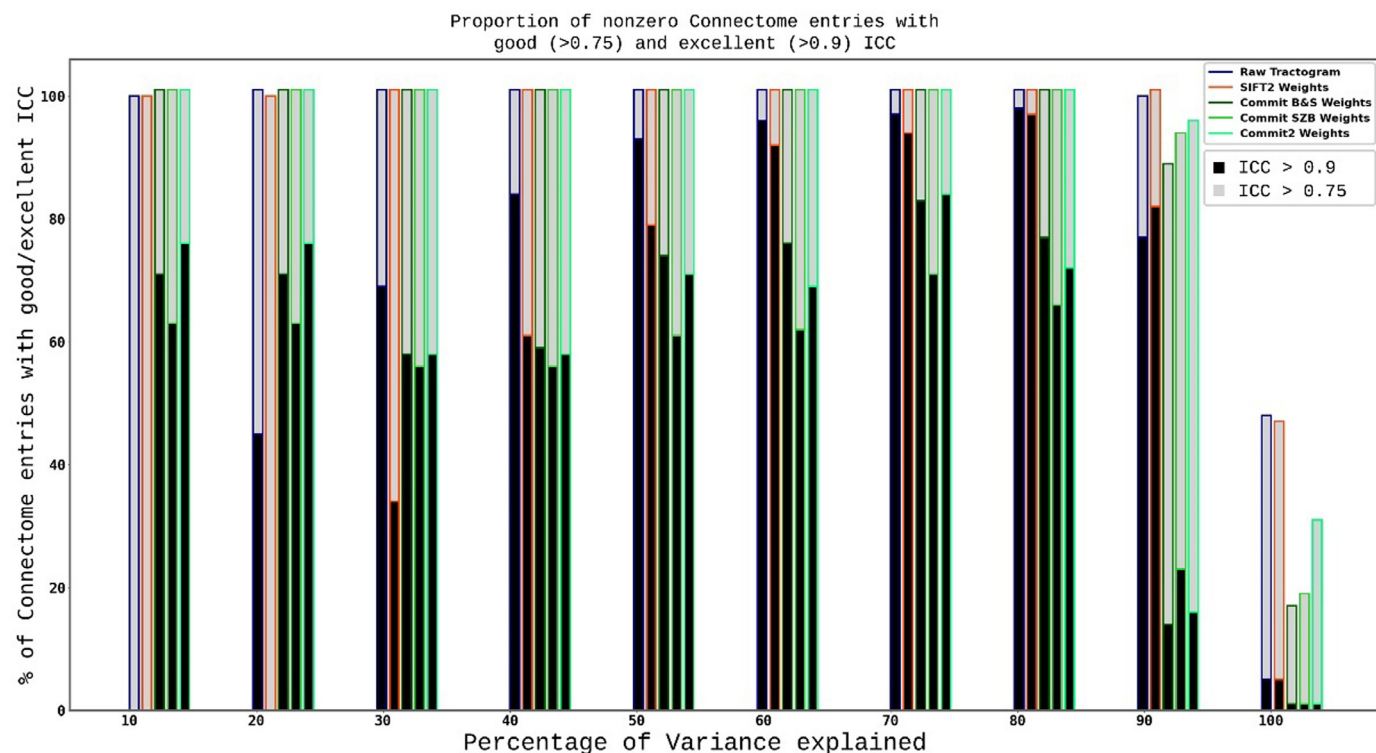

Fig. 3. The intraclass correlation coefficient (ICC) was generated for each entry of the connectome, considering only those entries without zero connectivity. This was done for the raw tractogram, the *SIFT2* filtered, the *COMMIT* (*B&S, SZB*) and *COMMIT2* filtered connectomes as well as the respective PCA-reduced connectomes (explained variance reaching from 10 to 90%). Of all considered entries, the proportion of those with ICC >0.75 and ICC>0.9 are shown, representing good and excellent reproducibility, respectively. Please note, that for 100% of the variance, no PCA was performed, but results for the raw tractograms and filtered tractograms are shown.

inter-session dissimilarity. For the whole-brain connectomes, the raw tractogram method depicts higher average interindividual dissimilarity and lower average intraindividual dissimilarity, compared to *SIFT2* and *COMMIT (see Table.Fig. 2.* The raw tractogram and the *SIFT2*-filtered one showed similar results regarding the bundle connectivity vectors, while *COMMIT* shows higher values. The average inter-run dissimilarity corresponds to 71.7% of the average inter-site dissimilarity. On the

other hand, the increase in the dissimilarity for the inter-session dataset corresponds to 19.8% of the average inter-site dissimilarity. Finally, the mean increase in the dissimilarity for the inter-site dataset corresponds to 8.5% of the total dissimilarity when comparing datasets of the same subject. Overall, the inter-run dissimilarity (same subject, scanner, and session) shows the highest percentage of dissimilarity when comparing the repeatability of all methods. This result is confirmed

Table 2

Repeated measure ANOVAs comparing mean intra and interindividual dissimilarities between site, session and run for the five evaluated whole-brain reconstruction methods separately.

Method	F-value	Uncorrected p-value	Partial eta-square effect size	Greenhouse-Geisser epsilon factor
Raw Tractogram	1.462263	0.209474	0.071461	0.329294
SIFT2	2.440955	0.039749	0.113845	0.385287
COMMIT B&S	0.35161	0.88006	0.01817	0.37194
COMMIT SZB	0.562517	0.728459	0.028755	0.385971
COMMIT2	0.63016	0.67715	0.03210	0.40486
Average FA	0.03341	0.99941	0.00176	0.45108
Average MD	0.13643	0.98349	0.00713	0.46065

Table 3

Average Bray-Curtis dissimilarity index comparing intraindividual dissimilarities between sites, sessions and runs for whole-brain connectomes and bundle connectivity vectors using the raw tractograms, *SIFT2*, *COMMIT* (Ball and Stick, and Stick, Zeppelin, Ball models) and *COMMIT2*. The dissimilarity index of the mean fractional anisotropy (FA) and mean diffusivity (MD) is also reported. Please note that the inter-session dissimilarity also includes the inter-run dissimilarity. Similarly, the inter-site dissimilarity also includes the inter-session dissimilarity.

Method		Average Bray-Curtis dissimilarity index		
		Inter-site	Inter-session	Inter-run
Whole-brain	**Raw Tractogram**	0.0927	0.0856	0.0677
Connectome	*SIFT2*	0.0916	0.0845	0.0651
	COMMIT B&S	0.1022	0.0977	0.0788
	COMMIT SZB	0.1003	0.0954	0.0770
	COMMIT2	0.1161	0.1102	0.0922
Bundle	**Raw Tractogram**	0.0618	0.0540	0.0438
Connectivity	*SIFT2*	0.0576	0.0545	0.0410
Vector	*COMMIT B&S*	0.0716	0.0617	0.0482
	COMMIT SZB	0.0679	0.0577	0.0457
	COMMIT2	0.0576	0.0545	0.0410
Diffusion	**Average FA**	0.0242	0.0216	0.0159
Tensor	**Average MD**	0.0198	0.0186	0.0136

when considering only the raw diffusion signal, represented as tensor (FA, MD).

3.2. Track-density imaging

Fig. 4A depicts the z-score map computed from the mean weighted track-density imaging (TDI) map. The distribution of the z-score for the white matter volume is shown in Fig. 4B. High positive z-score values (red) indicate regions of over-representation of the white matter trajectories, and increased negative z-score values (blue) indicate regions of underrepresentation. Voxel of white matter tissue should ideally show similar values. The raw tractogram and the *SIFT2* weighting methods show high z-scores values in the deep white matter. *SIFT2* shows a slight reduction in high z-score values compared to the raw tractogram. *COMMIT* methods showed a further decrease in high z-score voxels in the deep white matter. However, higher z-score values are noticeable in regions of single fibre populations (e.g., intern capsule, corpus callosum). Interestingly, filtering methods showed an increased z-score in the cerebellum (Fig. 4A bottom row), suggesting an underrepresentation in this region by the raw tractogram. Moreover, the z-scores produced by the *COMMIT* methods are more equally distributed in this region, which is not the case for other methods, particularly the raw tractogram. Fig. 4B also shows an increase in high negative z-scores for the *COMMIT* methods. These values are located at the grey matter and white matter boundaries, likely in voxels with partial volume contamination. The raw tractogram and *SIFT2* also estimated high negative z-score values in those voxels. Please see Supplementary Figure 2 for averaged TDI maps of the whole group for each reconstruction method without applying z-transformation. Further, the averaged TDI map of one single subject, and for one site, session and run was computed. Finally, the difference

between one individuum and the group average, as well as the difference between one run and one individuum, is represented.

3.3. Normal distribution of weights

For every white matter fascicle weight estimated at every repetition, the distribution of the structural connectivity estimates was evaluated within the studied cohort using the Shapiro Wilk test (Shapiro and Wilk, 1965). The percentage of normal distribution of the 29 fascicle weights is 10.2%, 55.6%, 45.4%, 50.0% and 47.2% for the raw tractogram, *SIFT2, COMMIT* (*B&S, SZB*) and *COMMIT2*, respectively. This suggests that microstructure-informed tractography reduces connectivity weights biases and provides more fascicles with normally distributed weights across the population.

4. Discussion

Microstructure-informed tractography methods have been introduced to address the specificity-sensitivity trade-off in tractography by reducing false-positive connections and adding biological meaning to reconstructed streamlines. Analyses in synthetic models of white-matter fascicles have proven high accuracy for *SIFT2* and *COMMIT* (Daducci et al., 2014b; Smith et al., 2015). Although, the validation is the bottleneck of tractography-based connectivity estimation algorithms. Previous studies used simplified phantoms with connectivity patterns much simpler than those observed in human brains. As an alternative validation approach, some studies focused on studying the reproducibility and repeatability of the estimated connectivity matrices. For example, the reproducibility of white matter reconstruction has been investigated comparing the acquisition and local diffusion models (Dayan et al., 2015; Gigandet et al., 2013; Prčkovska et al., 2016; Roine et al., 2019; Schumacher et al., 2018; Zhao et al., 2015), different tractography methods (Bonilha et al., 2015; Girard et al., 2020; Thomas et al., 2014), thresholding approaches (Colon-Perez et al., 2016; Konopleva et al., 2020; Roine et al., 2019) weighting of white matter pathways (Smith et al., 2015b), and differences in cortical and subcortical brain parcellations (Besson et al., 2014; Zhang et al., 2019). With the lack of ground truth data, the biological accuracy of estimated structural connectivity must be evaluated differently. Firstly, a robust tractography reconstruction must be reproducible. As such, the connectivity of large white matter bundles of a healthy population is expected to follow a normal distribution. Secondly, it must be biologically meaningful, i.e., representing key aspects of human brain anatomy. Thirdly, a valid reconstruction needs to be sensitive to individual differences, i.e., estimates need subject specificity. Finally, there is a need to investigate the influences on white matter reconstruction caused by differences between runs, sessions, and scanners to characterize the stability of the measurements and analyses. This is especially important when studying structural connectivity alterations in clinical applications, like in longitudinal studies with repetitive measurements, as findings can only be detected (and interpreted) when exceeding the intrinsic variability of the measurement itself, and large multi-centre studies are optimal if the employed methods do not show scanner and location bias.
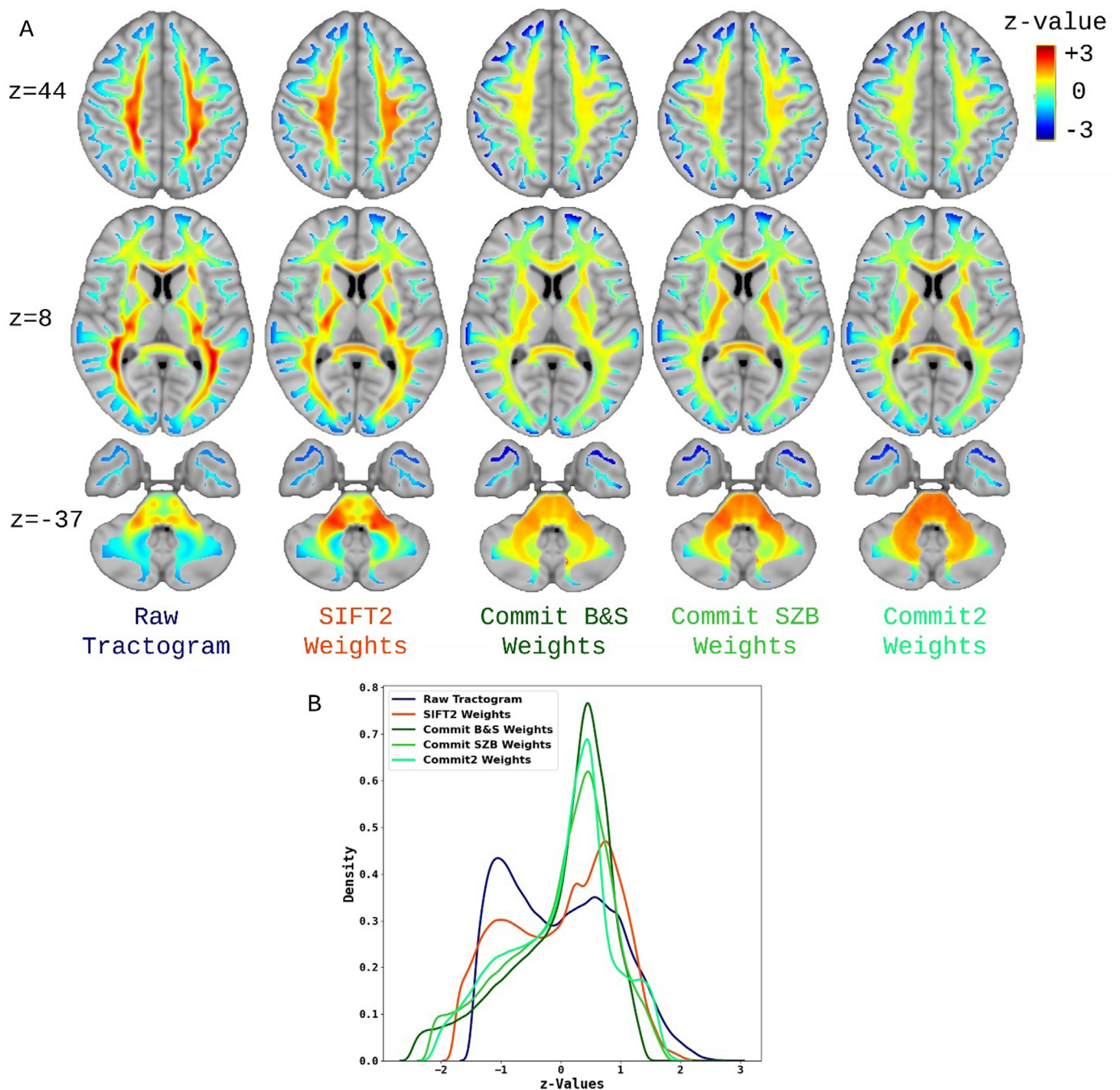
Fig. 4. Comparison of group mean weighted TDI maps of microstructure-informed tractography methods. A: TDI-maps were created using the raw tractogram and considering the weighting by the microstructure-informed tractography methods. All values were z-transformed, indicating the variance of structural connectivity over the whole-brain. An average map was created over all 160 datasets and presented on MNI standard brain (z-indices of horizontal slices given). B: The density plot shows the frequency of certain z-values.

In neuroimaging, reducing and quantifying variability is a necessity for translational research and for applying potential findings in clinical settings, especially in the view that longitudinal changes are crucially important in the understanding, monitoring and predicting of neurological disorders such as, e.g., stroke (Guggisberg et al., 2019; Koch et al., 2021; Koch and Hummel, 2017). Further, being sensitive to individual structural connectivity differences reflects the accuracy of white matter estimates. Evaluating the different impacts on reproducibility by site, time or run offers the possibility to pinpoint the greatest influence to guide further investigations. Finally, the quantification of the degree of uncertainties allows the translation to neuroscientific and clinical questions, expecting a significantly higher effect size than the noise level

found in pure intraindividual and interindividual variability. Thus, in this study, we evaluate the reproducibility and repeatability of white matter reconstruction and microstructure-informed tractography methods considering the effects of site, time and run. We evaluated those differences within the whole-brain connectomes and 29 large white matter bundles.

4.1. Subject-specificity and reproducibility for whole-brain structural connectivity

The whole-brain connectomes constructed by using the raw streamlines were highly subject-specific. High interindividual and low intrain-

dividual dissimilarities and maximal scores in seven-nearest-neighbours clustering were obtained (see Fig. 1, Table 1). This surprising result indicates that already the reconstruction of the raw connectome, despite its potentially high incidence of false-positive connections and biases, represents a highly specific individual profile. Tractography is known to be susceptible to false-positive and spurious streamlines, but those streamlines seem to capture subject specificity. In other words, this suggests that the false-positive streamlines are not random trajectories but dependant on the subjects' anatomy. When using microstructure-informed tractography methods, the subject specificity of connectomes remains high, as indicated by a high ratio of inter-subject and intraindividual dissimilarity as well as a high score in seven-nearest-neighbours clustering (see Fig. 1, Table 1).

The reproducibility of the connectome reconstruction was evaluated further by means of ICC (see Fig. 3). Here, the raw tractogram, *SIFT2* and *COMMIT2* weighted reveal reasonable levels of good reproducibility, whereas *COMMIT* modelling seems to be inferior. Still, when applying PCA to the connectome reconstruction, the reproducibility increases significantly, showing good to excellent reproducibility in all methods of reconstruction. Interestingly, especially *COMMIT* filtering shows excellent reproducibility even with low levels of variance explained. In this context, the PCA seems to filter the connectome reconstruction further, that individual connectome profiles gain stability while enhancing the separation of the individual reconstructions. These results support the usage of methods to reduce redundancy and collinearity for connectome reconstruction.

4.2. Bundle connectivity vectors

Considering the reconstruction of the 29 bundles, the application of microstructure-informed tractography methods is superior to results from the raw streamline with respect to inter-subject and intra-subject dissimilarity. This implies that adding microstructure information to the estimation of structural connectivity shows high subject specificity while remaining biologically meaningful connectivity estimates. Although, it was not possible to successfully identify every subject using the connectivity of the white matter bundles.

Investigating the structural connectivity within these bundles in the studied cohort suggested a substantial deviation from a normal distribution for most of the fascicles when considering the raw tractogram (10%, normally distributed). After applying microstructure-informed tractography, the connectivity distribution at the group level normalizes up to 50–55%. Even though there is no ground truth data, imaging studies and developing studies suggest a normal distribution of white matter fascicles (Lebel et al., 2019). The observed shift of distribution in the reconstructed white matter bundles is most likely by putting high weights on valid trajectories and low weights on invalid or redundant trajectories by the studied filtering methods. This might indicate a higher biological meaning. Future studies are needed to investigate the distribution of white matter fascicles in the human brain. This becomes especially important when investigating individual deviation of structural connectivity in neurological and psychiatric diseases.

4.3. PCA-reduced connectomes

Reducing the dimensionality of the whole-brain connectomes increases the inter-subject to intraindividual dissimilarity ratio with an optimum at 80% of the explained variance with approximatively 15 eigenvectors (raw tractogram: 16, *SIFT2*: 15, *COMMIT B&S*: 16, *COMMIT SZB*: 15, *COMMIT2*: 15) while maintaining a 100% success rate of seven-nearest-neighbour clustering (see Fig. 2). Further, the ICC gains excellent reproducibility after the application of PCA (se Fig. 3). This implies that not all elements of the whole-brain connectome are needed to identify individuals. Another explanation might be that PCA denoises the connectome elevating the biological meaning. This result

withholds novel and exciting possibilities for future connectome analyses. With 15 eigenvectors more complex statistical analyses are possible without losing too many degrees of freedom, while maintaining a high subject specificity. Surprisingly, when reducing the amount of variance explained by the used eigenvectors even further the *COMMIT* filtered connectomes maintain a high interindividual to intraindividual dissimilarity ratio. In contrast, the ratio decreases for the raw tractogram and the *SIFT2* method. This implies that even subcomponents of the connectome obtained using *COMMIT* methods show high subject specificity.

4.4. Estimation of white matter density

The standardized mean TDI maps (see Fig. 4) show the distribution of estimated streamlines density throughout the white matter and reflect key pitfalls in the reconstruction. High positive z-scores in the healthy white matter represent an oversampled density bias estimated from tractography. Areas of convergence of multiple fibre populations are vulnerable to those types of errors, being, e.g., the internal capsule and the corpus callosum. Microstructure-informed tractography methods reduced the overestimation especially prominent in the deep white matter (upper row), the internal capsule (middle row). Negative z-scores represent two aspects. On the one hand, voxels containing grey matter are expected to have lower white matter volume and thereby streamline density. On the other hand, low z-values within deep white matter voxels represent an underestimation of streamline density. Areas of high complex fibre architecture including crossing and kissing configurations are vulnerable to these types of errors, i.e., the pons and projection fibres with the cerebellum. The qualitative inspection of filtered tractograms TDI maps within the pons and the cerebellar white matter clearly shows a dense distribution of white matter fibers. In contrast, there is a bias on the trajectory of the corticospinal pathways and the cerebellar peduncle and a low density within the pons and the cerebellar white matter in the map obtained from the raw tractogram. Using microstructure-informed tractography, most voxels with negative z-scores seem to be on the white matter and grey matter boundary, as expected.

4.5. Source of structural connectivity variability

The impact of location, timepoint and run was evaluated. It was hypothesized that the intraindividual dissimilarity between datasets is the most sensitive to potential influences and variability of the acquisition and reconstruction. The repeated measure ANOVA revealed no differences in the dissimilarity scores between the data acquisitions; 7.1%, 11%, 1,8%, 2.9% and 3.2% of the total variance were attributed to the factor site, session and run when considering the raw tractogram, SIFT2, *COMMIT* (*B&S, SZB*) and *COMMIT2,* respectively (see Table 2). The maximum intraindividual dissimilarity was 0.1161 for the whole-brain connectomes and 0.0716 for the bundle connectivity vectors (see Table 3). Most of the intraindividual dissimilarity is associated to the inter-run dissimilarity (72,5% on average) rather than to the inter-site dissimilarity (8.8% on average) or the inter-session (18.7% on average) dissimilarity. This surprising result underpins the great reproducibility of structural connectivity, especially when considering time and site. Still, this raised the question of the source of the run variability. Repeating the analysis not using the reconstructed streamlines, but the mean of FA and MD maps derived from the diffusion tensor model confirms that the greatest source of dissimilarity is between runs (69.2% on average, see Table 3). This emphasizes that the acquisition of the DW-MRI data (used by the diffusion tensor model) is a high source of dissimilarity between runs. The processing algorithms like tractography or microstructure-informed tractography do not add much to the dissimilarity. Deviations from this natural variability thus mark a true biological difference, highlighting its meaning for systems neuroscience.

4.6. The structural connectivity fingerprint

Using the whole-brain connectome, seven-nearest-neighbour successfully clustered all datasets belonging to the same subject, i.e., the whole-brain connectivity profile is unique and reliable to identify an individual subject, such as a fingerprint. This was already shown for functional connectivity (Amico and Goñi, 2018; Finn et al., 2015; Van De Ville et al., 2021), particularly in the frontoparietal network. Moreover, the structural connectome is highly subject-specific (Yeh et al., 2016), with 100% subject classification performances using an alternative structural connectivity pipeline.

4.7. Limitations

Several aspects have to be mentioned limiting the conclusions of the given analyses. A generalisation of the results on the reproducibility is limited by the assessment in only two sites using the same scanner and acquisition protocol. Showing reproducibility in total independence of the scanner is needed (Kurokawa et al., 2021). In addition, the algorithm for tractography nor the set of streamlines or the cortical parcellation was altered, which can impact the reconstruction of connectomes and white matter bundles. Also, lower quality data, such as single shell local reconstruction like e.g. diffusion tensor imaging, was not considered in this study and is still often used for clinical research questions. Thus, future work is needed to explore its reproducibility. Finally, all results were based on the multi-tissue constrained spherical deconvolution method, and other alternative techniques are available (e.g., see (Canales-Rodríguez et al., 2019, 2015; Daducci et al., 2014a)).

5. Conclusion

Surprisingly, the raw tractogram shows high subject specificity at the connectome level, though its biological interpretation is limited. Microstructure-informed tractography shows high subject specificity as well as group reproducibility on connectome level and bundle connectivity vectors. By reducing high fibre density selectively in areas of fibre convergence architecture, microstructure-informed tractography increases the biological meaning of white matter reconstructions. Moreover, reducing the dimensionality of the data through PCA increases the subject specificity and represents a promising analysis step to be included when dealing with whole-brain connectomes. Finally, the largest amount of intraindividual variance arrives from inter-run comparison, most likely by the diffusion signal itself and not by the connectivity analysis. Time and site have a small influence on the variability. These results are fundamentally important considering the design and results of translational neuroscience and patient work and supporting cross-centre clinical data analyses. Findings exceeding the natural intrinsic variability may mark true biological meaning.

Credit author statement

PJK, GG, JB, AD, TK, FCH, JPH formulated the research goals and aims; PJK, GG, JB, MP, EJCR, EFG, SS, AD, GFP, TH, TK, JPT, FCH design the methodology and analysed the data; PJK, JB, AGCM, EB, CHP, TM, MJW collected the data; PJK, GG, JB wrote the original draft; PJK, GG, MP, EJCR, EFG, GFP, TH, TK, FCH reviewed and edited the manuscript; FCH, JPH acquired the financial support to perform the study.

Conflict of interest

G.F.P., T.H., and T.K. are employees of Siemens Healthcare AG, Switzerland.

Acknowledgements

Supplementary materials

Supplementary material associated with this article can be found, in the online version, at doi:10.1016/j.neuroimage.2022.119356.

References

Alexander, D.C., 2008. A general framework for experiment design in diffusion MRI and its application in measuring direct tissue-microstructure features. Magn. Reson. Med. 60, 439–448. doi:10.1002/mrm.21646.

Amico, E., Goñi, J., 2018. The quest for identifiability in human functional connectomes. Sci. Rep. 81 (8), 1–14. doi:10.1038/s41598-018-25089-1, 2018.

Andersson, J.L.R., Jenkinson, M., Smith, S., 2010. Non-linear registration aka Spatial normalisation, FMRIB Technial Report TR07JA2.

Andersson, J.L.R., Skare, S., Ashburner, J., 2003. How to correct susceptibility distortions in spin-echo echo-planar images: application to diffusion tensor imaging. Neuroimage 20, 870–888. doi:10.1016/S1053-8119(03)00336-7.

Andersson, J.L.R., Sotiropoulos, S.N., 2016. An integrated approach to correction for off-resonance effects and subject movement in diffusion MR imaging. Neuroimage 125, 1063–1078. doi:10.1016/j.neuroimage.2015.10.019.

Assaf, Y., Johansen-Berg, H., Thiebaut de Schotten, M., 2017. The role of diffusion MRI in neuroscience. NMR Biomed. 1–16. doi:10.1002/nbm.3762.

Barakovic, M., Girard, G., Schiavi, S., Romascano, D., Descoteaux, M., Granziera, C., Jones, D.K., Innocenti, G.M., Thiran, J.-.P., Daducci, A., 2021a. Bundle-specific axon diameter index as a new contrast to differentiate white matter tracts. Front. Neurosci. 0, 687. doi:10.3389/FNINS.2021.646034.

Barakovic, M., Romascano, D., Dyrby, T., Alexander, D., Descoteaux, M., Jean-Philippe Thiran, A.D., 2016. Assessment of bundle-specific axon diameter distributions using diffusion MRI tractography. Organization for Human Brain Mapping (HBM'16). Geneva, Switzerland.

Barakovic, M., Tax, C.M.W., Rudrapatna, U., Chamberland, M., Rafael-Patino, J., Granziera, C., Thiran, J.P., Daducci, A., Canales-Rodríguez, E.J., Jones, D.K., 2021b. Resolving bundle-specific intra-axonal T2 values within a voxel using diffusion-relaxation tract-based estimation. Neuroimage 227, 117617. doi:10.1016/j.neuroimage.2020.117617.

Besson, P., Lopes, R., Leclerc, X., Derambure, P., Tyvaert, L., 2014. Intra-subject reliability of the high-resolution whole-brain structural connectome. Neuroimage 102, 283–293. doi:10.1016/j.neuroimage.2014.07.064.

Bonilha, L., Gleichgerrcht, E., Fridriksson, J., Breedlove, J.L., Rorden, C., Nesland, T., Paulus, W., Helms, G., Focke, N.K., 2015. Reproducibility of the structural brain connectome derived from diffusion tensor imaging. PLoS ONE 10, 1–17. doi:10.1371/journal.pone.0135247.

Bray, J.R., Curtis, J.T., 1957. An ordination of the upland forest communities of southern wisconsin. Ecol. Monogr. 27, 325–349. doi:10.2307/1942268.

Calamante, F., Tournier, J.-.D., Jackson, G.D., Connelly, A., 2010. Track-density imaging (TDI): super-resolution white matter imaging using whole-brain track-density mapping. Neuroimage 53, 1233–1243. doi:10.1016/j.neuroimage.2010.07.024.

Canales-Rodríguez, E.J., Daducci, A., Sotiropoulos, S.N., Caruyer, E., Aja-Fernández, S., Radua, J., Mendizabal, J.M.Y., Iturria-Medina, Y., Melie-García, L., Alemán-Gómez, Y., Thiran, J.P., Sarró, S., Pomarol-Clotet, E., Salvador, R., 2015. Spherical deconvolution of multichannel diffusion MRI data with non-Gaussian noise models and spatial regularization. PLoS ONE 10. doi:10.1371/journal.pone.0138910.

Canales-Rodríguez, E.J., Legarreta, J.H., Pizzolato, M., Rensonnet, G., Girard, G., Patino, J.R., Barakovic, M., Romascano, D., Alemán-Gómez, Y., Radua, J., Pomarol-Clotet, E., Salvador, R., Thiran, J.P., Daducci, A., 2019. Sparse wars: a survey and comparative study of spherical deconvolution algorithms for diffusion MRI. Neuroimage 184, 140–160. doi:10.1016/j.neuroimage.2018.08.071.

Colon-Perez, L.M., Couret, M., Triplett, W., Price, C.C., Mareci, T.H., 2016. Small worldness in dense and weighted connectomes. Front. Phys. 4. doi:10.3389/FPHY.2016.00014.

Daducci, A., Canales-Rodríguez, E.J., Descoteaux, M., Garyfallidis, E., Gur, Y., Lin, Y.-.C., Mani, M., Merlet, S., Paquette, M., Ramirez-Manzanares, A., Reisert, M., Reis Rodrigues, P., Sepehrband, F., Caruyer, E., Choupan, J., Deriche, R., Jacob, M., Menegaz, G., Prčkovska, V., Rivera, M., Wiaux, Y., Thiran, J.-.P., 2014a. Quantitative

comparison of reconstruction methods for intra-voxel fiber recovery from diffusion MRI. IEEE Trans. Med. Imag. 33, 384–399. doi:10.1109/TMI.2013.2285500.

Daducci, A., Dal Palu, A., Lemkaddem, A., Thiran, J.-.P., 2014b. COMMIT: convex Optimization Modeling for Micro-structure Informed Tractography. IEEE Trans. Med. Imag. 34.

Daducci, A., Dal Palu, A., Lemkaddem, A., Thiran, J.-.P., 2013. A convex optimization framework for global tractography. In: IEEE International Symposium on Biomedical Imaging. IEEE, San Francisco, CA, USA, pp. 524–527. doi:10.1109/ISBI.2013.6556527.

Dayan, M., Kreutzer, S., Clark, C.A., 2015. Tractography of the optic radiation: a repeatability and reproducibility study. NMR Biomed 28, 423–431. doi:10.1002/NBM.3266.

Destrieux, C., Fischl, B., Dale, A., Halgren, E., 2010. Automatic parcellation of human cortical gyri and sulci using standard anatomical nomenclature. Neuroimage 53, 1–15. doi:10.1016/j.neuroimage.2010.06.010.

Finn, E.S., Shen, X., Scheinost, D., Rosenberg, M.D., Huang, J., Chun, M.M., Papademetris, X., Constable, R.T., 2015. Functional connectome fingerprinting: identifying individuals based on patterns of brain connectivity. Nat. Neurosci. 18, 1664. doi:10.1038/NN.4135.

Fischl, B., Salat, D.H., Busa, E., Albert, M., Dieterich, M., Haselgrove, C., van der Kouwe, A., Killiany, R., Kennedy, D., Klaveness, S., Montillo, A., Makris, N., Rosen, B., Dale, A.M., 2002. Whole brain segmentation: automated labeling of neuroanatomical structures in the human brain. Neuron 33, 341–355.

Fischl, B., van der Kouwe, A., Destrieux, C., Halgren, E., Ségonne, F., Salat, D.H., Busa, E., Seidman, L.J., Goldstein, J., Kennedy, D., Caviness, V., Makris, N., Rosen, B., Dale, A.M., 2004. Automatically parcellating the human cerebral cortex. Cereb. Cortex 14, 11–22. doi:10.1093/cercor/bhg087.

Frigo, M., Deslauriers-Gauthier, S., Parker, D., Aziz Ould Ismail, A., John Kim, J., Verma, R., Deriche, R., 2020. Diffusion MRI tractography filtering techniques change the topology of structural connectomes. J. Neural Eng. 17, 065002. doi:10.1088/1741-2552/abc29b.

Garyfallidis, E., Brett, M., Amirbekian, B., Rokem, A., Van Der Walt, S., Descoteaux, M., Nimmo-smith, I., Contributors, D., 2014. Dipy, a library for the analysis of diffusion MRI data. Front. Neuroinform. 8, 1–5.

Gigandet, X., Griffa, A., Kober, T., Daducci, A., Gilbert, G., Connelly, A., Hagmann, P., Meuli, R., Thiran, J.P., Krueger, G., 2013. A connectome-based comparison of diffusion MRI schemes. PLoS ONE 8. doi:10.1371/journal.pone.0075061.

Girard, G., Caminiti, R., Battaglia-Mayer, A., St-Onge, E., Ambrosen, K.S., Eskildsen, S.F., Krug, K., Dyrby, T.B., Descoteaux, M., Thiran, J.P., Innocenti, G.M., 2020. On the cortical connectivity in the macaque brain: a comparison of diffusion tractography and histological tracing data. Neuroimage 221, 117201. doi:10.1016/J.NEUROIMAGE.2020.117201.

Guggisberg, A.G., Koch, P.J., Hummel, F.C., Buetefisch, C.M., 2019. Brain networks and their relevance for stroke rehabilitation. Clin. Neurophysiol. 130, 1098–1124. doi:10.1016/j.clinph.2019.04.004.

Iglesias, J.E., Van Leemput, K., Bhatt, P., Casillas, C., Dutt, S., Schuff, N., Truran-Sacrey, D., Boxer, A., Fischl, B., 2015. Bayesian segmentation of brainstem structures in MRI. Neuroimage 113, 184–195. doi:10.1016/J.NEUROIMAGE.2015.02.065.

Jenkinson, M., Bannister, P., Brady, M., Smith, S., 2002. Improved optimization for the robust and accurate linear registration and motion correction of brain images. Neuroimage 17, 825–841.

Jeurissen, Ben, Tournier, Jacques-Donald, Dhollander, Thijs, Connelly, Alan, Sijbers, Jan, 2014. Multi-tissue constrained spherical deconvolution for improved analysis of multi-shell diffusion MRI data. Neuroimage 103, 411–426. doi:10.1016/J.NEUROIMAGE.2014.07.061.

Kaden, E., Kruggel, F., Alexander, D.C., 2015. Quantitative mapping of the per-axon diffusion coefficients in brain white matter. Magn. Reson. Med. 75, 1752–1763.

Kellner, E., Dhital, B., Kiselev, V.G., Reisert, M., 2016. Gibbs-ringing artifact removal based on local subvoxel-shifts. Magn. Reson. Med. 76, 1574–1581. doi:10.1002/MRM.26054.

Koch, P.J., Hummel, F.C., 2017. Toward precision medicine: tailoring interventional strategies based on noninvasive brain stimulation for motor recovery after stroke. Curr. Opin. Neurol. 30, 388–397. doi:10.1097/WCO.0000000000000462.

Koch, P.J., Park, C.-.H., Girard, G., Beanato, E., Egger, P., Evangelista, G.G., Lee, J., Wessel, M.J., Morishita, T., Koch, G., Thiran, J.-.P., Guggisberg, A.G., Rosso, C., Kim, Y.-.H., Hummel, F.C., 2021. The structural connectome and motor recovery after stroke: predicting natural recovery. Brain 144, 2107–2119. doi:10.1093/brain/awab082.

Konopleva, L., Il'yasov, K.A., Teo, S.J., Coenen, V.A., Kaller, C.P., Reisert, M., 2020. Robust intra-individual estimation of structural connectivity by principal component analysis. Neuroimage 226, 117483. doi:10.1016/j.neuroimage.2020.117483.

Kurokawa, R., Kamiya, K., Koike, S., Nakaya, M., Uematsu, A., Tanaka, S.C., Kamagata, K., Okada, N., Morita, K., Kasai, K., Abe, O., 2021. Cross-scanner reproducibility and harmonization of a diffusion MRI structural brain network: a traveling subject study of multi-b acquisition. Neuroimage 245, 118675. doi:10.1016/j.neuroimage.2021.118675.

Lebel, C., Treit, S., Beaulieu, C., 2019. A review of diffusion MRI of typical white matter development from early childhood to young adulthood. NMR Biomed 32, e3778. doi:10.1002/NBM.3778.

Maier-Hein, K.H., Neher, P.F., Houde, J.C., Côté, M.A., Garyfallidis, E., Zhong, J., Chamberland, M., Yeh, F.C., Lin, Y.C., Ji, Q., Reddick, W.E., Glass, J.O., Chen, D.Q., Feng, Y., Gao, C., Wu, Y., Ma, J., Renjie, H., Li, Q., Westin, C.F., Deslauriers-Gauthier, S., González, J.O.O., Paquette, M., St-Jean, S., Girard, G., Rheault, F., Sidhu, J., Tax, C.M.W., Guo, F., Mesri, H.Y., Dávid, S., Froeling, M., Heemskerk, A.M., Leemans, A., Boré, A., Pinsard, B., Bedetti, C., Desrosiers, M., Brambati, S., Doyon, J., Sarica, A., Vasta, R., Cerasa, A., Quattrone, A., Yeatman, J., Khan, A.R., Hodges, W., Alexander, S., Romascano, D., Barakovic, M., Auría, A., Esteban, O., Lemkaddem, A., Thiran, J.P., Cetingul, H.E., Odry, B.L., Mailhe, B., Nadar, M.S., Pizzagalli, F.,

Prasad, G., Villalon-Reina, J.E., Galvis, J., Thompson, P.M., Requejo, F.D.S., Laguna, P.L., Lacerda, L.M., Barrett, R., Dell'Acqua, F., Catani, M., Petit, L., Caruyer, E., Daducci, A., Dyrby, T.B., Holland-Letz, T., Hilgetag, C.C., Stieltjes, B., Descoteaux, M., 2017. The challenge of mapping the human connectome based on diffusion tractography. Nat. Commun. 8. doi:10.1038/s41467-017-01285-x.

Ocampo-Pineda, M., Schiavi, S., Rheault, F., Girard, G., Petit, L., Descoteaux, M., Daducci, A., 2021a. Hierarchical microstructure informed tractography. Brain Connect. doi:10.1089/brain.2020.0907, brain.2020.0907.

Pestilli, F., Yeatman, J.D., Rokem, A., Kay, K.N., Wandell, B.A., 2014. Evaluation and statistical inference for human connectomes. Nat. Methods 11, 1058–1063. doi:10.1038/nmeth.3098.

Prčkovska, V., Rodrigues, P., Puigdellivol Sanchez, A., Ramos, M., Andorra, M., Martinez-Heras, E., Falcon, C., Prats-Galino, A., Villoslada, P., 2016. Reproducibility of the Structural Connectome Reconstruction across Diffusion Methods. J. Neuroimag. 26, 46–57. doi:10.1111/JON.12298.

Reisert, M., Kiselev, V.G., Dihtal, B., Kellner, E., Novikov, D.S., 2014. MesoFT: Unifying Diffusion Modelling and Fiber Tracking, in: Medical Image Computing and Computer-Assisted Intervention (MICCAI'14). Boston, United-States, pp. 201–208. doi:10.1007/978-3-319-10443-0_26.

Roine, T., Jeurissen, B., Perrone, D., Aelterman, J., Philips, W., Sijbers, J., Leemans, A., 2019. Reproducibility and intercorrelation of graph theoretical measures in structural brain connectivity networks. Med. Image Anal. 52, 56–67. doi:10.1016/J.MEDIA.2018.10.009.

Sagi, Y., Tavor, I., Hofstetter, S., Tzur-Moryosef, S., Blumenfeld-Katzir, T., Assaf, Y., 2012. Learning in the fast lane: new insights into neuroplasticity. Neuron 73, 1195–1203. doi:10.1016/j.neuron.2012.01.025.

Schiavi, S., Ocampo-Pineda, M., Barakovic, M., Petit, L., Descoteaux, M., Thiran, J.P., Daducci, A., 2020a. A new method for accurate in vivo mapping of human brain connections using microstructural and anatomical information. Sci. Adv. 6, eaba8245. doi:10.1126/sciadv.aba8245.

Schilling, K.G., Gao, Y., Stepniewska, I., Janve, V., Landman, B.A., Anderson, A.W., 2019. Anatomical accuracy of standard-practice tractography algorithms in the motor system - a histological validation in the squirrel monkey brain. Magn. Reson. Imaging 55, 7–25. doi:10.1016/j.mri.2018.09.004.

Scholz, J., Klein, M.C., Behrens, T.E.J., Johansen-Berg, H., 2009. Training induces changes in white-matter architecture. Nat. Neurosci. 12, 1370–1371. doi:10.1038/nn.2412.

Schumacher, L., Reisert, M., Nitschke, K., Egger, K., Urbach, H., Hennig, J., Weiller, C., Kaller, C., 2018. Probing the reproducibility of quantitative estimates of structural connectivity derived from global tractography. Neuroimage 175, 215–229. doi:10.1016/J.NEUROIMAGE.2018.01.086.

Shapiro, S.S., Wilk, M.B., 1965. An Analysis of Variance Test for Normality (Complete Samples). Biometrika 52 (No. 3/4), 591–611. doi:10.2307/2333709.

Sherbondy, A.J., Rowe, M.C., Alexander, D.C., 2010. MicroTrack: an algorithm for concurrent projectome and microstructure estimation. In: Medical Image Computing and Computer-Assisted Intervention. Beijing, China, pp. 183–190.

Smith, C.A.B., 1957. On the estimation of intraclass corelation. Ann. Hum. Genet. 21, 363–373. doi:10.1111/J.1469-1809.1972.TB00291.X.

Smith, R.E., Tournier, J.-.D., Calamante, F., Connelly, A., 2013a. SIFT: spherical-deconvolution informed filtering of tractograms. Neuroimage 67, 298–312. doi:10.1016/j.neuroimage.2012.11.049.

Smith, R.E., Tournier, J.-.D., Calamante, F., Connelly, A., 2013b. SIFT: spherical-deconvolution informed filtering of tractograms. Neuroimage 67, 298–312.

Smith, R.E., Tournier, J.-D.D., Calamante, F., Connelly, A., 2015. SIFT2: enabling dense quantitative assessment of brain white matter connectivity using streamlines tractography. Neuroimage 119, 338–351. doi:10.1016/j.neuroimage.2015.06.092.

Smith, R.E., Tournier, J.D., Calamante, F., Connelly, A., 2015b. The effects of SIFT on the reproducibility and biological accuracy of the structural connectome. Neuroimage 104, 253–265. doi:10.1016/J.NEUROIMAGE.2014.10.004.

Smith, S.M., 2002. Fast robust automated brain extraction. Hum. Brain Mapp. 17, 143–155. doi:10.1002/hbm.10062.

Smith, S.M., Jenkinson, M., Woolrich, M.W., Beckmann, C.F., Behrens, T.E.J., Johansen-Berg, H., Bannister, P.R., De Luca, M., Drobnjak, I., Flitney, D.E., Niazy, R.K., Saunders, J., Vickers, J., Zhang, Y., De Stefano, N., Brady, J.M., Matthews, P.M., 2004. Advances in functional and structural MR image analysis and implementation as FSL. Neuroimage 23, S208–S219. doi:10.1016/J.NEUROIMAGE.2004.07.051.

Thomas, C., Ye, F.Q., Irfanoglu, M.O., Modi, P., Saleem, K.S., Leopold, D.A., Pierpaoli, C., 2014. Anatomical accuracy of brain connections derived from diffusion MRI tractography is inherently limited. Proc. Natl. Acad. Sci. 111, 16574–16579. doi:10.1073/PNAS.1405672111.

Tournier, J.-.D., Calamante, F., Connelly, A., 2007. Robust determination of the fibre orientation distribution in diffusion MRI: non-negativity constrained super-resolved spherical deconvolution. Neuroimage 35, 1459–1472.

Tournier, J.D., Smith, R., Raffelt, D., Tabbara, R., Dhollander, T., Pietsch, M., Christiaens, D., Jeurissen, B., Yeh, C.H., Connelly, A., 2019. MRtrix3: a fast, flexible and open software framework for medical image processing and visualisation. Neuroimage 202, 116137. doi:10.1016/j.neuroimage.2019.116137.

Van De Ville, D., Farouj, Y., Preti, M.G., Liégeois, R., Amico, E., 2021. When makes you unique: temporality of the human brain fingerprint. Sci. Adv. 7, 751–766. doi:10.1126/SCIADV.ABJ0751/SUPPL_FILE/SCIADV.ABJ0751_SM.PDF.

Wassermann, D., Makris, N., Rathi, Y., Shenton, M., Kikinis, R., Kubicki, M., Westin, C.-.F., 2016. The white matter query language: a novel approach for describing human white matter anatomy. Brain Struct. Funct. pp 1–17. doi:10.1007/s00429-015-1179-4.

Yeh, C.H., Smith, R.E., Liang, X., Calamante, F., Connelly, A., 2016. Correction for diffusion MRI fibre tracking biases: the consequences for structural connectomic metrics. Neuroimage 142, 150–162. doi:10.1016/j.neuroimage.2016.05.047.

Zhang, F., Wu, Y., Norton, I., Rathi, Y., Golby, A.J., O'Donnell, L.J., 2019. Test–retest reproducibility of white matter parcellation using diffusion MRI tractography fiber clustering. Hum. Brain Mapp 40, 3041–3057. doi:10.1002/HBM.24579.

Zhang, Y., Brady, M., Smith, S., 2001. Segmentation of brain MR images through a hidden Markov random field model and the expectation-maximization algorithm. IEEE Trans. Med. Imaging 20, 45–57. doi:10.1109/42.906424.

Zhao, T., Duan, F., Liao, X., Dai, Z., Cao, M., He, Y., Shu, N., 2015. Test-retest reliability of white matter structural brain networks: a multiband diffusion MRI study. Front. Hum. Neurosci. 0, 59. doi:10.3389/FNHUM.2015.00059.